Journal of Computational Physics **172,** 739–765 (2001)
doi:10.1006/jcph.2001.6856, available online at http://www.idealibrary.com on IDEAL®

A Tensor Artificial Viscosity Using a Mimetic Finite Difference Algorithm

J. C. Campbell*,[1] and M. J. Shashkov†

*T-7 and T-CNLS, Los Alamos National Laboratory, Los Alamos, New Mexico 87545; and †T-7, Los Alamos National Laboratory, Los Alamos, New Mexico 87545
E-mail: james@cnls.lanl.gov; shashkov@lanl.gov

Received October 5, 2000; revised April 18, 2001

We have developed a two-dimensional tensor artificial viscosity for finite difference shock wave computations. The discrete viscosity tensor is formed by multiplying the gradient of velocity tensor by a scalar term. The scalar term is based on the form of viscosity first presented by Kurapatanko, and also contains a limiter designed to switch off the viscosity for shockless compression and rigid-body rotation. Mimetic discretizations are used to derive the form of the momentum and energy equations for a nonorthogonal grid where the viscosity tensor is evaluated at the zone edges. The advantage of the tensor viscosity is a reduction of the dependence of the solution on the relation of the grid to the flow structure.

1. INTRODUCTION

In this paper we describe the implementation of a tensor artificial viscosity into a Lagrangian hydrodynamics code. The governing equations of Lagrangian hydrodynamics are the momentum (1) and energy equations (2), which are written

$$\rho \frac{d\mathbf{v}}{dt} = -\nabla P, \tag{1}$$

$$\rho \frac{de}{dt} = -P \nabla \cdot \mathbf{v}, \tag{2}$$

where ρ is density, P is pressure, e is specific internal energy, and $\mathbf{v}$ is the velocity vector.

If the hydrodynamics code is intended to solve problems containing shock waves, then special methods are required to model the shock wave; otherwise postshock oscillation will destroy the solution. A standard strategy is shock capturing through the introduction of an artificial viscosity term.

[1] Present address: School of Engineering, Cranfield University, Bedfordshire MKG3 OAL, United Kingdom.

0021-9991/01 $35.00

The methodology of artificial viscosity was first developed by Von Neumann and Richtmyer [18] for one-dimensional shock wave calculations. Their approach was to modify the momentum and energy equations by adding a dissipative, viscosity-like term to the pressure. This term was chosen to produce a shock wave thickness on the order of the spacing of the computational mesh. The Von Neumann–Richtmyer viscosity had the form

$$q = -c_q \rho \Delta \mathbf{v} |\Delta \mathbf{v}|, \tag{3}$$

where c_q is a nondimensional constant. This term is quadratic in $\Delta \mathbf{v}$, and is positive in compression and negative in expansion. The viscosity term is not required in expansion, and it is common to set $q = 0$ when $\Delta \mathbf{v} > 0$.

When using (3), nonphysical oscillations were still seen behind the shock wave. To remove these oscillations Landshoff [12] added a second term to q that was linear in $\Delta \mathbf{v}$ and so vanished less rapidly behind a shock wave. Now the viscosity has the form

$$q = c_L \rho c_s |\Delta \mathbf{v}| + c_Q \rho (\Delta \mathbf{v})^2, \tag{4}$$

where c_s is the local sound speed and c_L and c_Q are nondimensional constants, c_L multiplying the linear term, and c_Q the quadratic. This basic form of viscosity has become widely used.

Another form of the viscosity term was described by Wilkins [19] who attributed it to Kurapatenko [11], and which is derived from the expression for the pressure jump across a shock in an ideal gas,

$$q_{Kur} = \rho \left\{ c_2 \frac{(\gamma+1)}{4} |\Delta \mathbf{v}| + \sqrt{c_2^2 \left(\frac{\gamma+1}{4} \right)^2 (\Delta \mathbf{v})^2 + c_1^2 c_s^2} \right\} |\Delta \mathbf{v}| \tag{5}$$

where c_1 and c_2 are nondimensional constants, and γ is the ratio of specific heats. We refer to this expression as the Kurapatenko form of viscosity. With $c_1 = c_2 = 1$, ρ and c_s the density and sound speed ahead of the shock, and $\Delta \mathbf{v}$ the velocity jump across the shock, (5) gives the pressure jump across the shock. Equation (5) reduces to the linear term of the basic shock viscosity as $\Delta \mathbf{v} \to 0$, and the quadratic term as $c_s \to 0$ or when $\Delta \mathbf{v}$ becomes large.

In a one-dimensional calculation, $\Delta \mathbf{v}$ is clearly defined. The simplest extension to n dimensions is to treat the viscosity as a scalar pressure term and set $\Delta \mathbf{v} \approx \sqrt[n]{V}(\nabla \cdot \mathbf{v})$, where V is the zone volume. A more accurate extension would be to take the velocity jump across the zone in the direction of the shock, but reliably calculating the shock direction is difficult. For a review of viscosity formulations, see Benson [1].

Recently Caramana *et al.* [7] specified five properties that an artificial viscosity should possess; these include

1. Dissipativity: The artificial viscosity must only act to decrease kinetic energy.
2. Galilean invariance: The viscosity should not be affected by the addition of a constant velocity field, and should vanish smoothly as the velocity field becomes constant.
3. Self-similar motion invariance: The viscosity should vanish for uniform contraction and rigid rotation.
4. Wave-front invariance: The viscosity should have no effect along a wave front of constant phase.

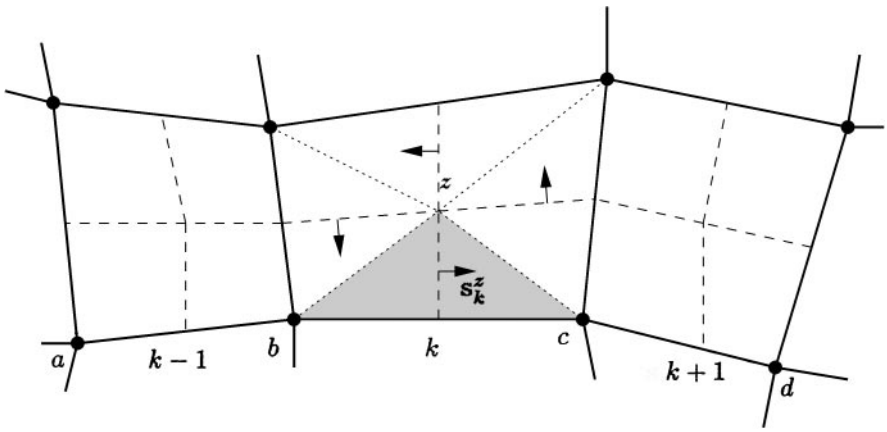

FIG. 1. A section of a logical mesh. The dotted lines show the boundaries of the triangular subzones, one subzone is shaded. The dashed lines show the median mesh. The vectors normal to the median mesh, s, are defined as positive in the direction shown. Edges $k-1$ and $k+1$ are the left and right neighbors of edge k in the limiter function.

5. Viscous force continuity: The viscous force should go to zero continuously as compression vanishes and remain zero for expansion.

In the same paper [7], an edge viscosity for Lagrangian codes designed to satisfy these conditions is then presented, although wave front invariance is only demonstrated for grids aligned with the flow, such as radial flow on a polar grid. Since we will compare our new viscosity to this edge viscosity, we now give a short description of the edge viscosity.

The edge viscosity assumes a spatially staggered grid where pressure, density, and energy are specified in the zones and velocity at the points. Each zone is subdivided by the median mesh that connects the center of a zone to the middle of each adjacent edge; see Fig. 1. The median mesh defines the control volume used to calculate the nodal forces in the momentum equation. The vector s is the normal to the median mesh; its magnitude is equal to the length of the associated piece of the median mesh.

For the edge viscosity, each zone is split into four triangular subzones, where each subzone is defined by the two nodes on an edge and the zone center; see Fig. 1. The viscosity is assumed constant inside each subzone. The nodal acceleration can then be calculated using the compatible finite difference method of integrating around the median mesh surrounding each node [5]. The median mesh around a point forms an eight-sided figure and the viscosity is assumed constant along each side.

Edge k connects the two points b and c in Fig. 1. For the subzone in zone z associated with edge k, the viscosity force is

$$\mathbf{f}_k^z = \begin{cases} (1-\psi_k) q_{Kur,k} \left(\widehat{\Delta \mathbf{v}}_k \cdot \mathbf{s}_k^z\right) \widehat{\Delta \mathbf{v}}_k & \text{if } \left(\Delta \mathbf{v}_k \cdot \mathbf{s}_k^z\right) < 0 \\ 0 & \text{if } \left(\Delta \mathbf{v}_k \cdot \mathbf{s}_k^z\right) \geq 0\,. \end{cases} \tag{6}$$

The edge force $\mathbf{f}_k^z$ contributes to the total force at points b and c. The velocity difference along the edge is $\Delta \mathbf{v}_k = \mathbf{v}_b - \mathbf{v}_c$, and $\widehat{\Delta \mathbf{v}}_k$ is the unit vector in the direction of this velocity

difference. For the edge, the density and sound speed are

$$\rho_k = \frac{2\rho_b\rho_c}{\rho_b + \rho_c}, \quad c_{s,k} = \min(c_{s,b}, c_{s,c}). \tag{7}$$

The density and sound speed at a node are the volume-weighted averages of the surrounding zones. The final term to be defined is ψ_k, which is a limiter function that acts to switch off the viscosity for self-similar motion and along wave fronts of constant phase. The limiter function is defined as

$$\psi_k = \max[0, \min(0.5(r_{l,k} + r_{r,k}), 2r_{l,k}, 2r_{r,k}, 1)], \tag{8}$$

$$r_{r,k} = \frac{\Delta\mathbf{v}_{k+1} \cdot \widehat{\Delta\mathbf{v}}_k}{\Delta\mathbf{x}_{k+1} \cdot \widehat{\Delta\mathbf{x}}_k} \Big/ \frac{|\Delta\mathbf{v}_k|}{|\Delta\mathbf{x}_k|}, \quad r_{l,k} = \frac{\Delta\mathbf{v}_{k-1} \cdot \widehat{\Delta\mathbf{v}}_k}{\Delta\mathbf{x}_{k-1} \cdot \widehat{\Delta\mathbf{x}}_k} \Big/ \frac{|\Delta\mathbf{v}_k|}{|\Delta\mathbf{x}_k|}. \tag{9}$$

Figure 1 shows how the left and right edges are defined on a logical grid. On an unstructured grid, the neighbor edges are found by checking all edges that meet at a point, and then selecting the edge that forms the largest angle with the center edge.

The term ψ is a multidimensional form of a one-dimensional TVD advection limiter. The limiter switches off the viscosity when the second derivative of the velocity field is zero and has the advantage that the second derivative does not have to be calculated. The limiter ensures that the viscosity satisfies the conditions of self-similar motion invariance and wave front invariance.

Figure 2 shows results obtained by using the edge viscosity to simulate the cylindrical Noh problem [14], a common test problem for Lagrangian hydrodynamics codes, for two different initial grids. A volume of perfect gas is given an initial inward radial velocity with unit magnitude. A circular shock wave is generated at the center of convergence and propagates outward. In the analytic solution, the shock wave has a radius of 0.2 at time 0.6. Both grids assume symmetry planes along the coordinate axes. The correct result is seen for the initially polar grid, Fig. 2a, where the grid remains polar and is aligned with the flow throughout the calculation. On the initially square grid, Fig. 2b, jets form along the axes and

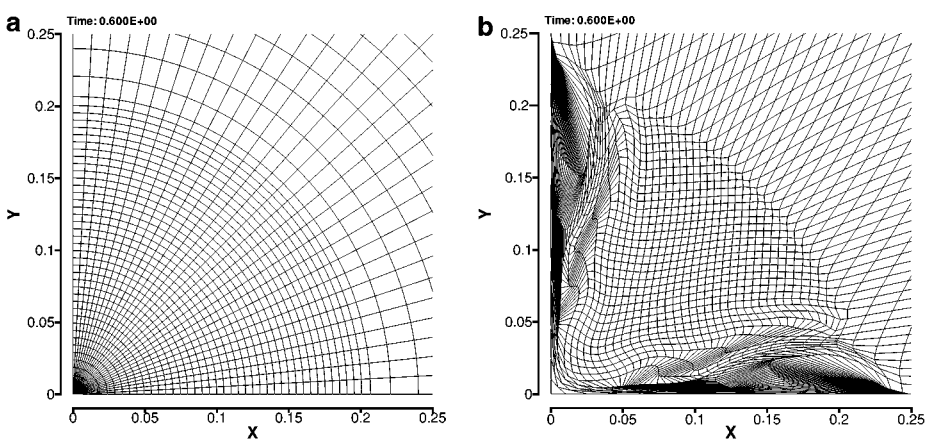

FIG. 2. Cylindrical Noh problem results for edge viscosity. (a) Polar grid, no subzonal pressures. (b) Cartesian grid, subzonal pressures merit factor $= 0.1$.

grid buckling occurs. The grid buckling can be controlled by using the subzonal pressure method [6]. This method uses subzonal forces to stabilize the grid by reducing spurious distortions. A nondimensional merit factor multiplies the magnitude of these forces; 0.1 is a small value for the merit factor. As can be seen in Fig. 2b, the use of subzonal pressures does prevent the grid buckling, but does not prevent the jets. The subzonal pressure method was only designed to suppress spurious grid motion at spatial scales equivalent to the local grid length. The jets occur on a larger spatial scale and are not suppressed. The jets are not caused by the boundary conditions, as the jets also occur when the whole domain is modeled.

Our opinion is that these jets occur as a result of the grid dependence of the edge viscosity. In [7], the edge viscosity is considered a local "tensor" that is constant within each triangular subzone. This "tensor" is formed from the product of the scalar factor $(1-\psi_k)q_{Kur,k}$, with the dyadic $\widehat{\Delta\mathbf{v}}_k\widehat{\Delta\mathbf{v}}_k$. However this "tensor" is not a discrete approximation of any continuous tensor. Even for a smooth flow on a smooth grid, the relative magnitude of its components can change dramatically within one zone because of the $\Delta\mathbf{v}$ term and the limiter function, which is designed to be directional. As a consequence, this viscosity does not have a well-defined continuum limit, and has a random dependence on the grid.

The aim of the work described here is to develop a viscosity that retains the useful features of the edge viscosity given by the five properties, but reduces the dependence on the relation of the grid to the flow structure. To achieve this we assume the viscosity is a discrete approximation of a continuous tensor function, $\mathbf{Q}$, which is a combination of a scalar coefficient and the gradient of velocity tensor. The viscous force is calculated in the momentum equation, which contains the divergence of tensor $\mathbf{Q}$. Choosing an artificial viscosity similar in analytical form to the physical viscosity tensor allows us to consider the derivation of the viscosity in two separate parts: the definition of the viscosity coefficient, and the derivation of discrete approximation to the gradient of velocity and the divergence of the viscosity tensor. As the artificial viscosity stress tensor does not have to be symmetric, we will consider a viscosity of the form

$$\mathbf{Q}=\mu\mathbf{G}^{\mathrm{T}}, \tag{10}$$

where $\mathbf{G}=\nabla\mathbf{v}$ and μ is a scalar coefficient. We will construct the discrete equations so that the viscosity tensor is calculated on zone edges as the tangential projection to the edge. This is natural for a staggered discretization where velocity components are given at grid nodes. As we will show by numerical experiment, our new viscosity, which we will refer to as "tensor viscosity", reduces the dependence of the numerical solution on the grid. The numerical experiments employ an unstructured grid finite difference code [3].

In the next section we will discuss the general form of the viscosity, and the constraints that must be placed on the form of the viscosity coefficient in order to satisfy the five properties of [7]. In Section 3, expressions for the divergence of a tensor and gradient of a vector in a general curvilinear coordinate system will be derived. These expressions will then be used in Section 4 to develop the discrete operators required to implement the tensor viscosity. Then in Section 5, we will describe the actual form of viscosity coefficient used, and the implementation of the viscosity in the test code. In Section 6, results from three test problems will be shown, comparing the edge viscosity to the new tensor viscosity. Finally, the conclusions will be given in Section 7.

2. CONTINUOUS FORM OF TENSOR ARTIFICIAL VISCOSITY

We introduce the general form of the new tensor viscosity and analyze it on the continuum level where the results are more transparent. We start by assuming a form similar to physical viscosity. However, it is not necessary for the artificial viscosity to be symmetric, so we use the gradient of velocity tensor, **G**, rather than the symmetric rate of deformation tensor used for physical viscosity. We define the viscosity tensor, **Q**, as

$$\mathbf{Q} = \mu \mathbf{G}^{\mathrm{T}}, \tag{11}$$

where μ is a scalar coefficient. For this viscosity tensor, the momentum and energy equations, considering only the viscosity terms, become

$$\rho \frac{d\mathbf{v}}{dt} = \nabla \cdot \mathbf{Q}^{\mathrm{T}} = \nabla \cdot (\mu \mathbf{G}) \tag{12}$$

$$\rho \frac{de}{dt} = \mathbf{Q} \cdot\cdot \mathbf{G} = \mu \mathbf{G} : \mathbf{G}, \tag{13}$$

where $\mathbf{Q} \cdot\cdot \mathbf{G} = Q_{ij} G_{ji}$, and $\mathbf{G} : \mathbf{G} = G_{ij} G_{ij}$ using the summation convention.

A nonsymmetric viscosity gives a useful property in the discrete model: there is no mode conversion [13]. This means that for a shear flow in which all velocities are parallel, the viscous force will only act in the velocity direction. With a symmetric tensor viscosity, the force would have a component perpendicular to the velocity direction.

In order to ensure dissipativity, we need to make sure that the viscosity can only decrease the kinetic energy. Therefore, in the energy equation we need to ensure that the $\mathbf{Q} \cdot\cdot \mathbf{G}$ is always positive. From (13) it can be seen that this condition is satisfied by ensuring $\mu \geq 0$.

Self-similar motion invariance requires that $\mu = 0$; this property can be achieved by including a limiter function similar to that used for the edge viscosity. Galilean invariance requires that μ is Galilean invariant. In addition, as the velocity field becomes constant, all terms in **G** must become zero, so the viscosity will vanish smoothly.

Viscous force continuity requires some switch to ensure that $\mu = 0$ in expansion. For the tensor viscosity, a clear choice for defining compression and expansion is the divergence of velocity. However, this switch will only partly satisfy the condition that the viscosity force should go to zero smoothly. It can be seen in Eq. (6) that the edge viscosity contains the $(\Delta \mathbf{v}_k \cdot \mathbf{s}_k^z)$ term that is used to detect compression and expansion. As this term multiplies all other terms in the force equation, it ensures that the force does go to zero smoothly. In the tensor viscosity, this property can only be satisfied by ensuring that μ goes to zero smoothly. This would require a quadratic only viscosity with the $\Delta \mathbf{v}$ term proportional to $\nabla \cdot \mathbf{v}$. The tensor viscosity can only fully satisfy this property at the expense of introducing oscillations behind a shock wave. We choose to use both linear and quadratic terms to suppress the oscillations, with the consequence that viscous force continuity is not satisfied.

The final property, wave-front invariance, is satisfied because of the functional form of viscosity, so the limiter function is only required to ensure self-similar motion invariance. To check for wave-front invariance, we will take the case of radial flow, which was used in [7] to show wave-front invariance for the edge viscosity. For 2D cylindrical coordinates (r, θ), the velocity gradient tensor is

$$\mathbf{Q} = \mu \begin{bmatrix} \frac{\partial v_r}{\partial r} & \frac{\partial v_\theta}{\partial r} \\ \frac{1}{r}\frac{\partial v_r}{\partial \theta} - \frac{v_\theta}{r} & \frac{1}{r}\frac{\partial v_\theta}{\partial \theta} + \frac{v_r}{r} \end{bmatrix}, \tag{14}$$

and the momentum equation is

$$\begin{aligned} \rho a_r &= \frac{\partial Q_{rr}}{\partial r} + \frac{1}{r}\frac{\partial Q_{\theta r}}{\partial \theta} + \frac{1}{r}(Q_{rr} - Q_{\theta\theta}) \\ \rho a_\theta &= \frac{\partial Q_{r\theta}}{\partial r} + \frac{1}{r}\frac{\partial Q_{\theta\theta}}{\partial \theta} + \frac{1}{r}(Q_{r\theta} - Q_{\theta r}). \end{aligned} \tag{15}$$

For radial flow, $v_\theta = 0$ and $\frac{\partial v_r}{\partial \theta} = 0$ so the momentum equation becomes

$$\begin{aligned} \rho a_r &= \frac{\partial}{\partial r}\left(\mu \frac{\partial v_r}{\partial r}\right) + \frac{\mu}{r}\frac{\partial v_r}{\partial r} \\ \rho a_\theta &= 0. \end{aligned} \tag{16}$$

As the viscosity only produces accelerations in the radial direction, it satisfies the condition of wave-front invariance.

3. GRADIENT OF A VECTOR AND DIVERGENCE OF A TENSOR IN A GENERAL COORDINATE SYSTEM

To implement the tensor viscosity, we need to define the discrete analogs of the divergence of a tensor and the gradient of a vector. To introduce limiters and retain the good properties of the edge viscosity, it will be useful to construct these discrete operators using a local coordinate system. This will allow the viscosity tensor to be defined by tangential projections to the zone edges in the discrete divergence operator. In this section, we derive continuous expressions for the divergence and gradient for a general coordinate system, which will be used as a guide to derive the discrete expressions.

We consider two coordinate systems. The first is the Cartesian coordinate system, (x, y). The second is a general curvilinear system, (ξ, η), with basis vectors $\mathbf{e}_\xi$ and $\mathbf{e}_\eta$ tangential to the coordinate lines. These are shown in Fig. 3. The Cartesian components of the basis vectors are

$$\mathbf{e}_\xi = \begin{pmatrix} \frac{\partial x}{\partial \xi} \\ \frac{\partial y}{\partial \xi} \end{pmatrix}, \quad \mathbf{e}_\eta = \begin{pmatrix} \frac{\partial x}{\partial \eta} \\ \frac{\partial y}{\partial \eta} \end{pmatrix}. \tag{17}$$

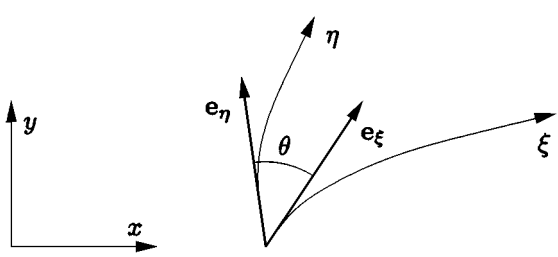

FIG. 3. Basis vectors of general coordinate system (ξ, η). θ is the angle between the vectors tangential to the coordinate system.

The components of the metric tensor relative to the general coordinate system are

$$g_{\xi\xi} = \mathbf{e}_\xi \cdot \mathbf{e}_\xi, \quad g_{\eta\eta} = \mathbf{e}_\eta \cdot \mathbf{e}_\eta, \quad g_{\xi\eta} = g_{\eta\xi} = \mathbf{e}_\eta \cdot \mathbf{e}_\xi. \tag{18}$$

From these the determinant of the metric tensor, $|g|$, can be found.

The gradient of velocity tensor, $\mathbf{G}$, is defined as

$$G_{ij} = \frac{\partial v_i}{\partial x_j}, \tag{19}$$

where $x_1 = x$, $x_2 = y$ and $\mathbf{v} = [v_1, v_2] = [v_x, v_y]$. For convenience, we write this as

$$\mathbf{G} = \text{grad}\, \mathbf{v} = \nabla \mathbf{v}. \tag{20}$$

In a general coordinate system, a tensor can be represented by two vectors that are projections of the tensor to the two basis vectors. Each vector is the dot product of the tensor with a unit basis vector

$$\mathbf{G}^\xi = \mathbf{G} \cdot \hat{\mathbf{e}}_\xi \quad \text{and} \quad \mathbf{G}^\eta = \mathbf{G} \cdot \hat{\mathbf{e}}_\eta, \tag{21}$$

where the hat signifies a unit vector. The Cartesian components of these vectors can be rewritten in terms of the derivatives of the vector $\mathbf{v}$ with respect to ξ and η

$$\mathbf{G}^\xi = \frac{1}{\sqrt{g_{\xi\xi}}} \begin{pmatrix} \frac{\partial v_x}{\partial \xi} \\ \frac{\partial v_y}{\partial \xi} \end{pmatrix} = \begin{pmatrix} \mathbf{G}^{\xi x} \\ \mathbf{G}^{\xi y} \end{pmatrix}, \quad \mathbf{G}^\eta = \frac{1}{\sqrt{g_{\eta\eta}}} \begin{pmatrix} \frac{\partial v_x}{\partial \eta} \\ \frac{\partial v_y}{\partial \eta} \end{pmatrix} = \begin{pmatrix} \mathbf{G}^{\eta x} \\ \mathbf{G}^{\eta y} \end{pmatrix}. \tag{22}$$

In the discrete case, we will derive the expression for the divergence, $\text{div}\, \mathbf{T} = \nabla \cdot \mathbf{T}$, using a discrete form of the integral identity

$$\int_V \nabla \mathbf{v} : \mathbf{T}\, dV = \oint_{\partial V} \mathbf{v} \cdot (\mathbf{T} \cdot \mathbf{n})\, dS - \int_V \mathbf{v} \cdot (\nabla \cdot \mathbf{T})\, dV, \tag{23}$$

where $\mathbf{T}$ is any second-order tensor. This expression means that the divergence is the negative adjoint of the gradient,

$$(\text{div}) = -(\text{grad})^*. \tag{24}$$

To use the identity (23), an expression for the tensor scalar product in terms of the tangential projections is required. The scalar product is easily written in terms of the Cartesian components of the tensors. We start by defining the Cartesian components of $\mathbf{G}$ in terms of $\mathbf{G}^\xi$ and $\mathbf{G}^\eta$. These formulae are valid for any tensor, and are found by solving the set of equations represented by (21)

$$\begin{aligned} G_{xx} &= \frac{\sqrt{g_{\xi\xi}}}{\sqrt{|g|}} \frac{\partial y}{\partial \eta} \mathbf{G}^{\xi x} - \frac{\sqrt{g_{\eta\eta}}}{\sqrt{|g|}} \frac{\partial y}{\partial \xi} \mathbf{G}^{\eta x} \\ G_{xy} &= \frac{\sqrt{g_{\eta\eta}}}{\sqrt{|g|}} \frac{\partial x}{\partial \xi} \mathbf{G}^{\eta x} - \frac{\sqrt{g_{\xi\xi}}}{\sqrt{|g|}} \frac{\partial x}{\partial \eta} \mathbf{G}^{\xi x} \end{aligned} \tag{25}$$

$$G_{yx} = \frac{\sqrt{g_{\xi\xi}}}{\sqrt{|g|}}\frac{\partial y}{\partial \eta}\mathbf{G}^{\xi y} - \frac{\sqrt{g_{\eta\eta}}}{\sqrt{|g|}}\frac{\partial y}{\partial \xi}\mathbf{G}^{\eta y}$$
$$G_{yy} = \frac{\sqrt{g_{\eta\eta}}}{\sqrt{|g|}}\frac{\partial x}{\partial \xi}\mathbf{G}^{\eta y} - \frac{\sqrt{g_{\xi\xi}}}{\sqrt{|g|}}\frac{\partial x}{\partial \eta}\mathbf{G}^{\xi y}.$$

Now it is possible to write the scalar product and collect terms to derive

$$\mathbf{G} : \mathbf{T} = \mathbf{G}^{\xi} \cdot \left[\mathbf{T}^{\xi}\frac{g_{\xi\xi}g_{\eta\eta}}{|g|} - \mathbf{T}^{\eta}\frac{g_{\xi\eta}}{|g|}\sqrt{g_{\xi\xi}}\sqrt{g_{\eta\eta}}\right] + \mathbf{G}^{\eta} \cdot \left[\mathbf{T}^{\eta}\frac{g_{\xi\xi}g_{\eta\eta}}{|g|} - \mathbf{T}^{\xi}\frac{g_{\xi\eta}}{|g|}\sqrt{g_{\xi\xi}}\sqrt{g_{\eta\eta}}\right]. \tag{26}$$

Rearranging and noting that

$$\frac{g_{\xi\xi}g_{\eta\eta}}{|g|} = \frac{1}{\sin^2\theta}, \quad \frac{g_{\xi\eta}}{\sqrt{g_{\xi\xi}}\sqrt{g_{\eta\eta}}} = \cos\theta \tag{27}$$

allows us to rewrite the scalar product only in terms of the tangential projections and the angle θ between $\mathbf{e}_{\xi}$ and $\mathbf{e}_{\eta}$ (Fig. 3):

$$\mathbf{G} : \mathbf{T} = \frac{1}{\sin^2\theta}[\mathbf{G}^{\xi} \cdot \mathbf{T}^{\xi} + \mathbf{G}^{\eta} \cdot \mathbf{T}^{\eta} - \cos\theta(\mathbf{G}^{\xi} \cdot \mathbf{T}^{\eta} + \mathbf{G}^{\eta} \cdot \mathbf{T}^{\xi})]. \tag{28}$$

Comparing (28) with the expression for the vector dot product in [9] shows that the two expressions are equivalent except that the ξ and η terms are vectors in this case.

In deriving an expression for the divergence using (23) we assume, for simplicity, that the surface integral is zero. Then we use Eq. (25) for $\nabla\mathbf{v} : \mathbf{T}$ and replace the $\mathbf{G}^{\xi}$ and $\mathbf{G}^{\eta}$ terms with the derivatives of vector $\mathbf{v}$ using (22). This gives

$$\int\int \nabla\mathbf{v}:\mathbf{T}\sqrt{|g|}\,d\xi\,d\eta$$
$$= \int\int \left(\frac{\partial \mathbf{v}}{\partial \xi} \cdot \left[\frac{\mathbf{T}^{\xi} - \cos\theta\mathbf{T}^{\eta}}{\sqrt{g_{\xi\xi}}\sin^2\theta}\right] + \frac{\partial \mathbf{v}}{\partial \eta} \cdot \left[\frac{\mathbf{T}^{\eta} - \cos\theta\mathbf{T}^{\xi}}{\sqrt{g_{\eta\eta}}\sin^2\theta}\right]\right)\sqrt{|g|}\,d\xi\,d\eta. \tag{29}$$

Integrating this expression by parts gives two terms that are equivalent to the RHS of (23). Ignoring the terms representing the surface integral leaves

$$\int\int \mathbf{v} \cdot (\nabla \cdot \mathbf{T})\sqrt{|g|}\,d\xi\,d\eta$$
$$= \int\int \left(\mathbf{v} \cdot \frac{\partial}{\partial \xi}\left[\sqrt{|g|}\frac{\mathbf{T}^{\xi} - \cos\theta\mathbf{T}^{\eta}}{\sqrt{g_{\xi\xi}}\sin^2\theta}\right] + \mathbf{v} \cdot \frac{\partial}{\partial \eta}\left[\sqrt{|g|}\frac{\mathbf{T}^{\eta} - \cos\theta\mathbf{T}^{\xi}}{\sqrt{g_{\eta\eta}}\sin^2\theta}\right]\right) d\xi\,d\eta. \tag{30}$$

Now we can write the expression for the divergence

$$\nabla \cdot \mathbf{T} = \frac{1}{\sqrt{|g|}}\left\{\frac{\partial}{\partial \xi}\left[\sqrt{|g|}\frac{\mathbf{T}^{\xi} - \cos\theta\mathbf{T}^{\eta}}{\sqrt{g_{\xi\xi}}\sin^2\theta}\right] + \frac{\partial}{\partial \eta}\left[\sqrt{|g|}\frac{\mathbf{T}^{\eta} - \cos\theta\mathbf{T}^{\xi}}{\sqrt{g_{\eta\eta}}\sin^2\theta}\right]\right\}. \tag{31}$$

This form can also be derived directly from the expression for the divergence in terms of T_{xx}, T_{yy}, T_{xy}, and T_{yx}. However, from a methodological point of view, it is useful to derive it using the integral identity.

4. DISCRETE OPERATORS

This section describes the derivation of discrete forms of the gradient of a vector and divergence of a tensor on a grid. The derivation uses tangential projections to zone edges, and is an extension of the mimetic finite difference method [9, 10, 17] to second-order tensors. In the mimetic finite difference method, a discrete approximation for a differential operator, such as divergence or gradient, is chosen. This initial or prime operator then supports the derivation of other discrete operators.

4.1. Grid

We construct the discrete functions on a spatially staggered grid. Figure 4a shows a section of the staggered grid. The median mesh is constructed by connecting the zone centers with the mid-side points. A fundamental assumption for a Lagrangian method is that each zone of the grid represents a discrete volume element that may deform, but does not gain or lose mass. If the zone center moves in a Lagrangian manner then the same assumption can be made for the median mesh. This justifies the definition of a Lagrangian subzonal corner volume, shown in Fig. 4a as the shaded area, which has constant mass. We denote the corner volume as V_p^z, where the indices denote the zone and point with which it is associated. We define $V_p^z = V_z^p$ and follow the convention that in a sum we always sum with respect to the lower index. The corner volume can then be used to define both a zone volume and a point volume:

$$V_z = \sum_{p \in S(z)} V_p^z, \quad V_p = \sum_{z \in S(p)} V_z^p \tag{32}$$

The stencil for a zone is each point that is a vertex of the zone. For a point, the stencil is every adjacent zone. As the mass of a subzone is constant, a density is easily defined for

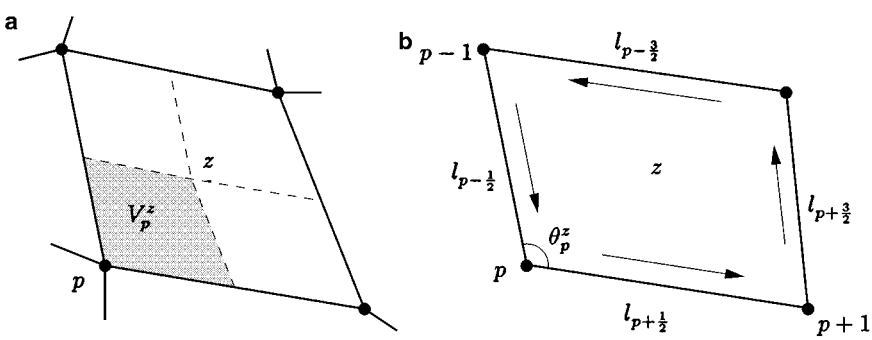

FIG. 4. (a) Fragment of a staggered grid, including zone z and point p. The solid lines show the grid and the dashed lines show the median mesh. The shaded area shows a subzonal Lagrangian corner object with volume V_p^z. (b) We choose notation relative to the currently selected point p, which is a vertex of zone z. The arrows next to each edge show the positive direction of $\hat{\mathbf{e}}$. The length of edge $p+\frac{1}{2}$ is $l_{p+\frac{1}{2}}$.

the volume. The same super and subscript notation is used for any value that is associated with both a point and a zone.

Figure 4b illustrates the notation used for the geometrical elements used in the discrete operators. The notation is relative to point p, which is a vertex of zone z. The expression $\hat{\mathbf{e}}_{p+\frac{1}{2}}$ is the unit vector along edge $p+\frac{1}{2}$, which connects points p and $p+1$. The arrows shown define the positive direction of $\hat{\mathbf{e}}$. The length of the edge $p+\frac{1}{2}$ is $l_{p+\frac{1}{2}}$. The expression θ_p^z is the angle between the two edges of zone z that meet at point p.

4.2. The Prime Operator

We need expressions for the following two operators: **GRAD**, the discrete form of the vector gradient, and **DIV**, the discrete form of the tensor divergence. In this paper, tensors are defined as tangential projections to the zone edges. We choose the discrete vector gradient as the prime operator.

For the direction given by unit vector $\hat{\mathbf{l}}$, the directional derivative of the vector field $\mathbf{v}$ is

$$\frac{\partial \mathbf{v}}{\partial l} = \hat{\mathbf{l}} \cdot \nabla \mathbf{v}. \tag{33}$$

Then the projection of this tensor $\mathbf{G} = \mathbf{GRAD}\ \mathbf{v}$ to the edge $p+\frac{1}{2}$ is

$$\mathbf{G}^e_{p+\frac{1}{2}} = \mathbf{G}_{p+\frac{1}{2}} \cdot \hat{\mathbf{e}}_{p+\frac{1}{2}} = \frac{\mathbf{v}_{p+1} - \mathbf{v}_p}{l_{p+\frac{1}{2}}}. \tag{34}$$

The relation between Eqs. (34) and (22) becomes clear when we recall the identities

$$dl_\xi = \sqrt{g_{\xi\xi}}\, d\xi, \quad dl_\eta = \sqrt{g_{\eta\eta}}\, d\eta, \tag{35}$$

where dl_ξ and dl_η are elements of the arcs of the coordinate curves.

4.3. The Derived Operator

We now use the prime operator to derive the discrete divergence **DIV**, through the definition $\mathbf{DIV} = -\mathbf{GRAD}^*$.

The first step is to construct a discrete form of Eq. (28), the tensor scalar product. We approximate the continuous equation by

$$\begin{aligned}(\mathbf{G}, \mathbf{T})_z \;=\; & \sum_{p \in S(z)} \frac{W_p^z}{\sin^2 \theta_p^z} \Big\{ \mathbf{G}^e_{p-\frac{1}{2}} \cdot \mathbf{T}^e_{p-\frac{1}{2}} + \mathbf{G}^e_{p+\frac{1}{2}} \cdot \mathbf{T}^e_{p+\frac{1}{2}} \\ & + \cos\theta_p^z \left[\mathbf{G}^e_{p-\frac{1}{2}} \cdot \mathbf{T}^e_{p+\frac{1}{2}} + \mathbf{G}^e_{p+\frac{1}{2}} \cdot \mathbf{T}^e_{p-\frac{1}{2}} \right] \Big\},\end{aligned} \tag{36}$$

which defines the scalar product in zone z. In this expression, the sign of the cosine has changed because of the sign convention adopted. The expression W_p^z are weights that satisfy the conditions

$$W_p^z \geq 0, \quad \sum_{p \in S(z)} W_p^z = 1. \tag{37}$$

We define W_p^z as one-half the area of the triangle in zone z that contains the angle at point p, divided by volume of the zone. For a nonquadrilateral zone, this definition must be normalized to ensure that the second condition is satisfied. This choice of weights gives a first-order approximation of the operator [17].

To derive **DIV** from (36) and (34), we use the discrete form of the integral identity (23) and assume for simplicity that the surface integral is zero. This gives us

$$\sum_z (\mathbf{G}, \mathbf{T})_z V_z = -\sum_p (\mathbf{v}, \mathbf{DIV}\ \mathbf{T})_p V_p. \tag{38}$$

Substitute (36) into (38), and substitute for $\mathbf{G}^e$ using (34). This gives an expression that contains the velocity vector at three points: $\mathbf{v}_{p+1}$, $\mathbf{v}_p$, and $\mathbf{v}_{p-1}$. Then rewriting the expression to collect all the $\mathbf{v}$ terms at point p gives

$$\begin{aligned}
&-\sum_p (\mathbf{v}, \mathbf{DIV}\ \mathbf{T})_p V_p \\
&\quad = \sum_z \sum_{p\in S(z)} \mathbf{v}_p \cdot \left(\frac{W_p^z}{\sin^2\theta_p^z} \left\{ \frac{\mathbf{T}^e_{p-\frac12}}{l_{p-\frac12}} - \frac{\mathbf{T}^e_{p+\frac12}}{l_{p+\frac12}} + \cos\theta_p^z \left[\frac{\mathbf{T}^e_{p+\frac12}}{l_{p-\frac12}} - \frac{\mathbf{T}^e_{p-\frac12}}{l_{p+\frac12}} \right] \right\} \right. \\
&\qquad \left. + \frac{W_{p-1}^z}{\sin^2\theta_{p-1}^z} \left\{ \frac{\mathbf{T}^e_{p-\frac12}}{l_{p-\frac12}} + \cos\theta_{p-1}^z \frac{\mathbf{T}^e_{p-\frac32}}{l_{p-\frac12}} \right\} - \frac{W_{p+1}^z}{\sin^2\theta_{p+1}^z} \left\{ \frac{\mathbf{T}^e_{p+\frac12}}{l_{p+\frac12}} + \cos\theta_{p+1}^z \frac{\mathbf{T}^e_{p+\frac32}}{l_{p+\frac12}} \right\} \right) V_z.
\end{aligned} \tag{39}$$

Now the expression for **DIV T** at a point can be found

$$\begin{aligned}
(\mathbf{DIV}\ \mathbf{T})_p \;=\; \frac{1}{V_p} \sum_{z\in S(p)} V_z \left[\frac{1}{l_{p+\frac12}} \left\{ \frac{W_z^{p+1}}{\sin^2\theta_z^{p+1}} \left(\mathbf{T}^e_{p+\frac12} + \cos\theta_z^{p+1} \mathbf{T}^e_{p+\frac32} \right) \right\} \right. \\
+ \frac{1}{l_{p+\frac12}} \left\{ \frac{W_z^p}{\sin^2\theta_z^p} \left(\mathbf{T}^e_{p+\frac12} + \cos\theta_z^p \mathbf{T}^e_{p-\frac12} \right) \right\} \\
- \frac{1}{l_{p-\frac12}} \left\{ \frac{W_z^p}{\sin^2\theta_z^p} \left(\mathbf{T}^e_{p-\frac12} + \cos\theta_z^p \mathbf{T}^e_{p+\frac12} \right) \right\} \\
\left. - \frac{1}{l_{p-\frac12}} \left\{ \frac{W_z^{p-1}}{\sin^2\theta_z^{p-1}} \left(\mathbf{T}^e_{p-\frac12} + \cos\theta_z^{p-1} \mathbf{T}^e_{p-\frac32} \right) \right\} \right].
\end{aligned} \tag{40}$$

Figure 5 shows the stencil for the operator $(\mathbf{DIV}\ \mathbf{T})_p$. In the derivation above we have made no assumptions about the grid structure. These operators are equally applicable for structured and unstructured grids [4].

5. DISCRETE FORM OF TENSOR ARTIFICIAL VISCOSITY

We now define the discrete scalar viscosity coefficient, μ, and combine it with the discrete divergence to produce an expression for the viscous force. In analogy with the edge viscosity, we base the definition on the Kurapatenko form (5). In order to satisfy the dissipativity

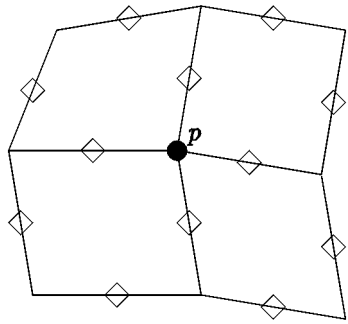

FIG. 5. Stencil for operator $(\mathbf{DIV}\,\mathbf{T})_p$ on a logically rectangular grid.

condition when using the discrete scalar product, (36), the viscosity coefficient must be constant within a corner volume. We define μ as

$$\mu_z^p = \left(1-\psi_z^p\right)\rho_z^p\left\{c_2\frac{(\gamma+1)}{4}\left|\Delta\mathbf{v}_z^p\right| + \sqrt{c_2^2\left(\frac{\gamma+1}{4}\right)^2\left(\Delta\mathbf{v}_z^p\right)^2 + c_1^2 {c_{s,z}}^2}\right\} l_z^p. \quad (41)$$

The speed of sound in zone z is $c_{s,z}$; c_1 and c_2 are nondimensional, nonnegative constants. The corner density, ρ_z^p, is easily defined as the corner volume is a Lagrangian.

We use the velocity divergence of the corner volume to detect compression and expansion. If the velocity divergence is positive in a corner, we set $\mu_z^p = 0$. The velocity divergence in a corner is defined as

$$\begin{aligned}(\nabla\cdot\mathbf{v})_z^p = \frac{1}{2V_z^p}\big[&(u_z-u_p)\left(y_{p-\frac{1}{2}}-y_{p+\frac{1}{2}}\right) - \left(u_{p-\frac{1}{2}}-u_{p+\frac{1}{2}}\right)(y_z-y_p)\\ &-(v_z-v_p)\left(x_{p-\frac{1}{2}}-x_{p+\frac{1}{2}}\right) + \left(v_{p-\frac{1}{2}}-v_{p+\frac{1}{2}}\right)(x_z-x_p)\big],\end{aligned} \quad (42)$$

where $\mathbf{v}=[u, v]$. The velocity for an edge is the average of the velocity at the two end points. The velocity of a zone is the average of the zone vertex velocities.

The viscosity coefficient requires a definition for the velocity jump, $\Delta\mathbf{v}_z^p$ and for the characteristic length, l_z^p. A length scale is required to ensure that the dimensions of the viscosity tensor are correct. The definition of these values has often caused difficulties in multidimensional shock viscosities [1]. Simple definitions of length, such as the square root of cell area in 2D, result in instabilities for large aspect ratio zones. Such zones do occur in practical problems. A more sophisticated approach is to determine the shock direction in a zone, but this has proved difficult to do accurately and reliably. This approach also has problems with large aspect ratio cells, where a small change in velocity or geometry can result in a large change in the length and velocity jump. To avoid these difficulties, we look for a characteristic length that varies smoothly in time, and does not overestimate the length.

A corner volume is adjacent to two edges, the lengths of which are $l_{p+\frac{1}{2}}$ and $l_{p-\frac{1}{2}}$; see Fig. 4. We define the length as

$$l_z^p = \min\left(l_{p+\frac{1}{2}}, l_{p-\frac{1}{2}}\right). \quad (43)$$

This choice of the smallest local length gives a measure that varies smoothly in time, is not too large in high aspect ratio zones, and it avoids the need to estimate the shock direction.

For the velocity jump we use

$$\Delta \mathbf{v}_z^p = l_z^p |\nabla \cdot \mathbf{v}|_z^p. \tag{44}$$

This term contains the corner velocity divergence that we use as the compression–expansion switch, and so it will go to zero smoothly as compression vanishes.

The final term to be defined is the limiter function ψ_z^p, which is calculated from the limiter values on the adjacent edges

$$\psi_z^p = \min\left(\psi_{p+\frac{1}{2}}, \psi_{p-\frac{1}{2}}\right). \tag{45}$$

For edge k the limiter function is

$$\psi_k = \min(\psi_1, \psi_2), \tag{46}$$

where

$$\begin{aligned} \psi_1 &= \max[0, \min(0.5(r_{l,k} + r_{r,k}), 2r_{l,k}, 2r_{r,k}, 1)] \\ \psi_2 &= \max[0, \min(0.5(r_{m,k} + r_{p,k}), 2r_{m,k}, 2r_{p,k}, 1)]. \end{aligned} \tag{47}$$

The r terms are defined

$$\begin{aligned} r_{l,k} &= \frac{(\mathbf{div}\ \mathbf{v})_l}{(\mathbf{div}\ \mathbf{v})_k}, \quad r_{r,k} = \frac{(\mathbf{div}\ \mathbf{v})_r}{(\mathbf{div}\ \mathbf{v})_k} \\ r_{a,k} &= \frac{(\mathbf{div}\ \mathbf{v})_a}{(\mathbf{div}\ \mathbf{v})_k}, \quad r_{b,k} = \frac{(\mathbf{div}\ \mathbf{v})_b}{(\mathbf{div}\ \mathbf{v})_k}. \end{aligned} \tag{48}$$

This limiter function requires four neighbor edges. In addition to the same left and right edges used for the edge viscosity, above a and below b edges must be chosen. Figure 6 shows how these neighbor edges are defined on a quadrilateral grid. For an edge, the divergence is calculated for the quadrilateral volume formed by the two end points and the centers of the two adjacent zones; see Fig. 6. In one dimension, this function reduces to the same function as the edge viscosity limiter.

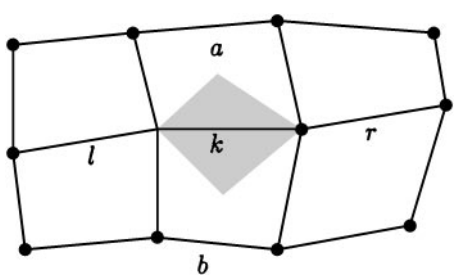

FIG. 6. Neighbor edges of edge k used for limiter function. The shaded area shows the volume used to calculate the divergence of velocity for the edge.

It is possible to define a similar function that calculates a limiter value directly for a corner volume, by using the velocity divergence calculated for corner volumes. However, this gives incorrect results because the velocity at three of the four vertices of a corner is interpolated. The limiter function will switch off the viscosity if all neighbor volumes have equal or larger divergence. The incorrect results can be clearly seen in the case when a shock wave is aligned with the grid, such as in a one-dimensional calculation. In this case, the corner limiter will switch off the viscosity for corners on the upstream side of a zone as the wave passes through the zone.

It is convenient to calculate the viscous force at a point in terms of corner forces, $\mathbf{f}_z^p$. A corner force is the force from zone z that acts on point p; so summing over the stencil of p gives the total force at the point. The discrete momentum equation at point p is written

$$m_p \frac{d\mathbf{v}_p}{dt} = V_p(\mathbf{DIV}\ \mathbf{Q})_p = \mathbf{F}_p = \sum_{z \in S(p)} \mathbf{f}_z^p, \tag{49}$$

where m_p is the point mass. The viscosity corner force $\mathbf{f}_z^p$ is then

$$\begin{aligned}
\mathbf{f}_z^p \;=\; V_z \Bigg[& \frac{1}{l_{p+\frac{1}{2}}} \left\{ \frac{W_z^{p+1}}{\sin^2 \theta_z^{p+1}} \left(\mu_z^{p+1} \mathbf{G}^e_{p+\frac{1}{2}} + \cos\theta_z^{p+1} \mu_z^{p+1} \mathbf{G}^e_{p+\frac{3}{2}} \right) \right\} \\
& + \frac{1}{l_{p+\frac{1}{2}}} \left\{ \frac{W_z^{p}}{\sin^2 \theta_z^{p}} \left(\mu_z^{p} \mathbf{G}^e_{p+\frac{1}{2}} + \cos\theta_z^{p} \mu_z^{p} \mathbf{G}^e_{p-\frac{1}{2}} \right) \right\} \\
& - \frac{1}{l_{p-\frac{1}{2}}} \left\{ \frac{W_z^{p}}{\sin^2 \theta_z^{p}} \left(\mu_z^{p} \mathbf{G}^e_{p-\frac{1}{2}} + \cos\theta_z^{p} \mu_z^{p} \mathbf{G}^e_{p+\frac{1}{2}} \right) \right\} \\
& - \frac{1}{l_{p-\frac{1}{2}}} \left\{ \frac{W_z^{p-1}}{\sin^2 \theta_z^{p-1}} \left(\mu_z^{p-1} \mathbf{G}^e_{p-\frac{1}{2}} + \cos\theta_z^{p-1} \mu_z^{p-1} \mathbf{G}^e_{p-\frac{3}{2}} \right) \right\} \Bigg].
\end{aligned} \tag{50}$$

For zone z, the discrete energy equation is

$$M_z \frac{de_z}{dt} = V_z(\mathbf{Q}, \mathbf{G})_z. \tag{51}$$

Then using (39) it can be shown that the discrete energy equation becomes

$$M_z \frac{de_z}{dt} = -\sum_{p \in S(z)} \mathbf{f}_p^z \cdot \mathbf{v}_p. \tag{52}$$

These expressions are the discrete analogs of the continuous equations in Section 3. Thus, they retain the properties of the continuous equations, such as dissipativity. Using the mimetic finite difference approach to derive these expressions ensures that total energy is conserved exactly, to numerical round off.

This viscosity only fully satisfies the viscous force continuity condition, that the viscous force should go to zero smoothly as compression vanishes, when the linear term is removed ($c_1 = 0$). However, when tested this removal resulted in oscillations behind shock waves, so we retain the linear term.

6. NUMERICAL RESULTS

We have implemented the tensor artificial viscosity in a test code. The test code [3] is a two-dimensional, plane strain, unstructured grid Lagrangian finite difference code that uses a compatible hydrodynamics algorithm [5]. The test code uses the Lagrangian subzonal pressure method to control grid distortion [6], and also contains the edge viscosity developed by Caramana *et al.* [7], which is briefly described in the introduction. Therefore, we have one code that contains both the edge viscosity and the tensor viscosity, allowing direct comparison of the effects of the two different viscosities.

To avoid any interaction of the subzonal pressures and the artificial viscosity that may obscure differences resulting from the different viscosities, subzonal pressures have not been used unless necessary. In the following results, no subzonal pressures were used unless otherwise indicated.

We present results for three test problems used to investigate the behavior of the tensor viscosity. In all problems, the viscosity coefficients were $c_1 = c_2 = 1.0$ for both viscosities.

6.1. Noh Implosion Problem

The Noh problem [14] is a well-known test problem for Lagrangian algorithms. Here the cylindrical implosion problem is modeled. A perfect gas with $\gamma = 5/3$ is given an initial unit inward radial velocity. A circular shock wave is generated at the center of convergence and subsequently expands. At time 0.6, this shock wave has a radial coordinate of 0.2, and the density behind the shock is 16.0. Ahead of the shock, the gas is compressed as a result of the convergence, and this produces a density profile with the equation $\rho = 1 + (t/R)$, where R is the radial coordinate and t the time. Results are shown for a polar grid (Fig. 7), and an initially Cartesian grid (Figs. 8–11).

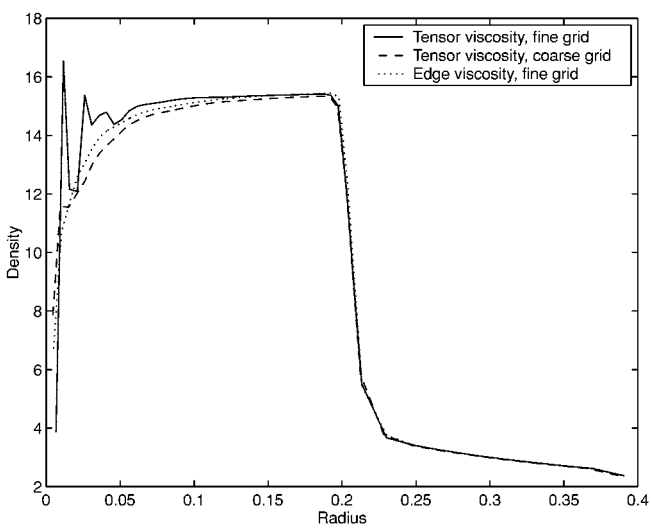

FIG. 7. Comparison of Noh problem results on a polar grid for tensor and edge viscosity. Both grids have 50 radial zones, initially all have an equal radial length of 0.02. The fine grid has 3° angular zoning, the coarse grid has 9° angular zoning. The zones at the origin have an aspect ratio of 6.4 : 1 for the coarse grid, and 19.1 : 1 for the fine grid.

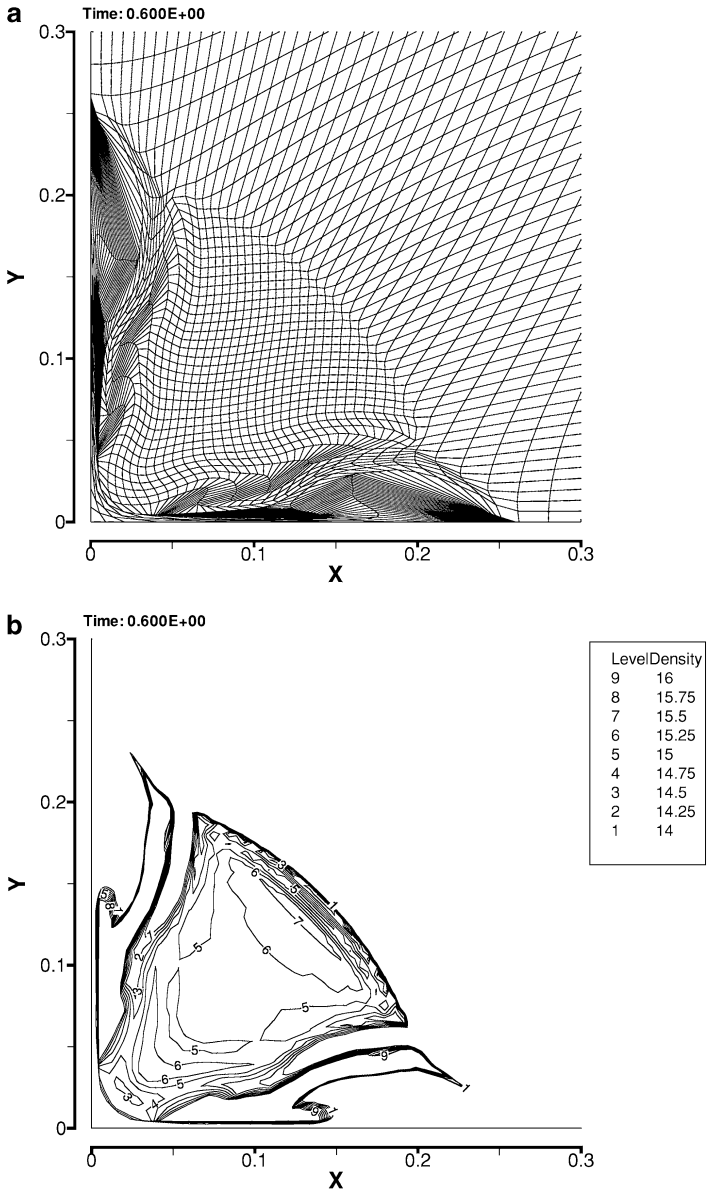

FIG. 8. Noh problem results on an initially Cartesian grid for edge viscosity, merit factor $= 0.1$. (a) Grid. (b) Density contour plot.

The polar grid is constructed with 50 zones in the radial direction, and a maximum radius of 1.0. The angular zoning is variable. The zones are quadrilateral away from the origin and triangular at the origin. An example of the grid can be seen in Fig. 2. On a polar grid, the edge viscosity gives better results (Fig. 7). This is due to the long thin zones at the point of convergence. As the polar grid is aligned to the flow, the limiter function ensures that the edge viscosity only acts along radial edges. With the tensor viscosity the uneven solution near the origin is caused by the characteristic length, which has large variation near the origin. It is possible to mitigate this problem by choosing a characteristic length

specifically for this grid, such as the length of the longer edges. However, this choice, on a fine polar grid, requires a very small time step to retain symmetry. In the tensor viscosity, each corner force is a vector with radial and tangential components; at a point, the tangential components cancel and leave a total force vector that is radial. If the characteristic length is large compared to the shortest zone edge, then the tangential components are large and round-off error combined with the low mass of the points close to the origin results in some tangential motion of these nodes. This motion can be controlled by choosing a restrictive time step; for 3° angular zoning, we found a CFL scale factor of ≤ 0.05 was required.

The Cartesian grid is 50×50 zones, and the overall length of each edge is 1.0. Only a quarter of the volume is modeled, symmetry boundary conditions are used along the x and y axes. This is a test problem where the edge viscosity fails (Fig. 8). Along the axes, jets form that result in a highly distorted grid and, without subzonal pressures, results in internal grid points passing through the symmetry planes. Consequently, subzonal pressures are required to reach time 0.6. However, subzonal pressures are not a cure for the problem, but do prevent zones inverting and do not allow grid points to pass through the symmetry planes. Increasing the merit factor results in the jets becoming even more pronounced. The grid can be improved by increasing the c_1 viscosity coefficient to around 3.75 or higher, but this causes an error in the shock location and a very uneven density behind the shock (Fig. 9).

For an initially square grid, the tensor viscosity results show a circular shock of radius 0.2, and a smooth grid behind the shock (Fig. 10). The density is not completely smooth behind the shock, as angular variations are seen. Near the 45° line there is an overshoot in the density immediately behind the shock, while no overshoot is observed near the coordinate axes. The variation in the density can be clearly seen in Fig. 11, which plots the density as a function of radius.

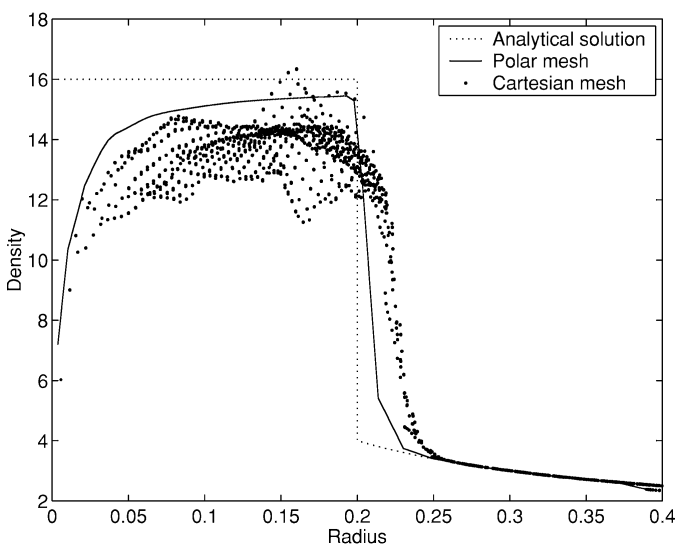

FIG. 9. Comparison of Noh problem results for polar ($c_1 = 1.0$) and Cartesian ($c_1 = 3.75$) grids for edge viscosity. For the Cartesian grid, each point is a zone density plotted for the radius of the zone center.

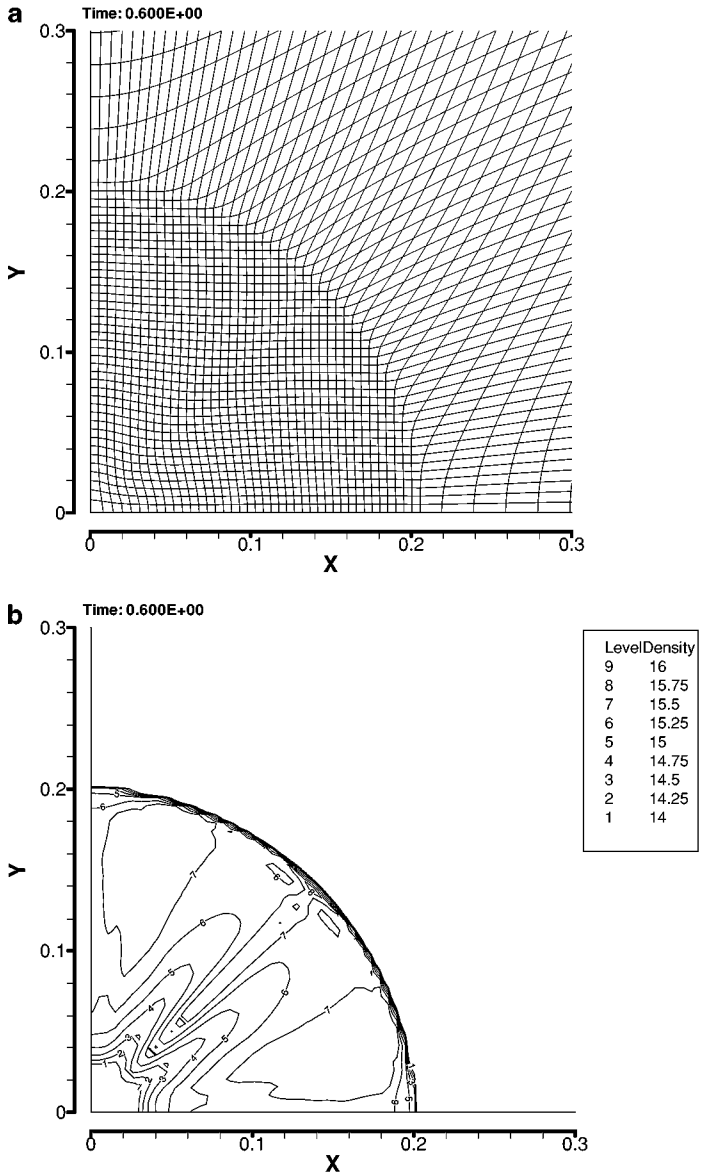

FIG. 10. Noh problem results on a Cartesian grid for tensor viscosity, no subzonal pressures. (a) Grid. (b) Density contour plot.

Results for both viscosities show the well-known wall heating problem; this appears in the density profile, which is underestimated near the point of convergence. We have not attempted to address this problem in the tensor viscosity as this is an inherent problem with shock physics codes [15], and approaches to treating wall heating are available [8, 14].

6.2. Saltzman Piston Problem

In the Saltzman piston problem [13] a one-dimensional shock wave propagates through a two-dimensional grid. This problem tests the ability of the code to model shock waves

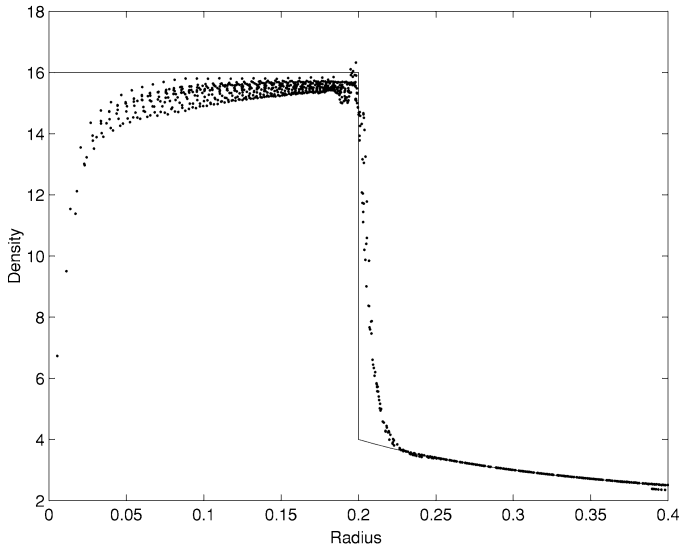

FIG. 11. Noh problem results for the tensor viscosity on a Cartesian grid, compared with the exact result. Each point is the density of a zone plotted against the radius of the zone center.

that are oblique to the grid. As artificial viscosity is critical for shock wave propagation, the Saltzman piston problem has often been used as in testing artificial viscosities [1, 2, 13].

In the Saltzman problem, one end of a gas-filled box is a piston. The piston moves into the box with a constant velocity of 1.0 and a strong shock wave is generated. The gas is described by an ideal gas equation of state with $\gamma = 5/3$. The initial grid is shown in Fig. 12. The initial length (x) is 1.0, and the height (y) is 0.1. The grid is 100 zones in the x-direction and 10 in the y-direction. On the upper and lower boundaries, symmetry boundary conditions are used. The nodal x coordinates are prescribed as a function of their logical coordinates i, j by

$$x(i,\ j) = (i-1)dx + (11-j)\sin\left(\frac{\pi(i-1)}{100}\right)dy, \tag{53}$$

where $dx = 1/100$ and $dy = 0.1/10$.

Results are shown for time 0.7 and time 0.925. At time 0.7, the analytic shock has an x-coordinate of 0.9333, and has not yet reached the fixed end. The density behind the shock is 4.0. By time 0.925, the shock has an x-coordinate of 0.95, and the shock has reflected off the fixed and then moving ends. Now the density ahead of the shock is 10.0 and the density behind the shock is 20.0. By this time, the grid ahead of the shock wave consists

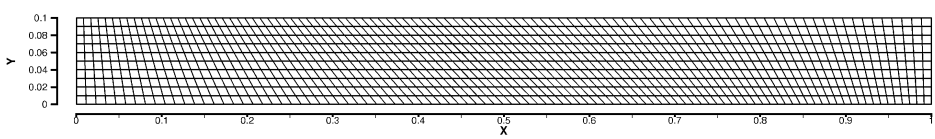

FIG. 12. Initial grid for Saltzman piston problem. The piston moves from left to right at constant velocity.

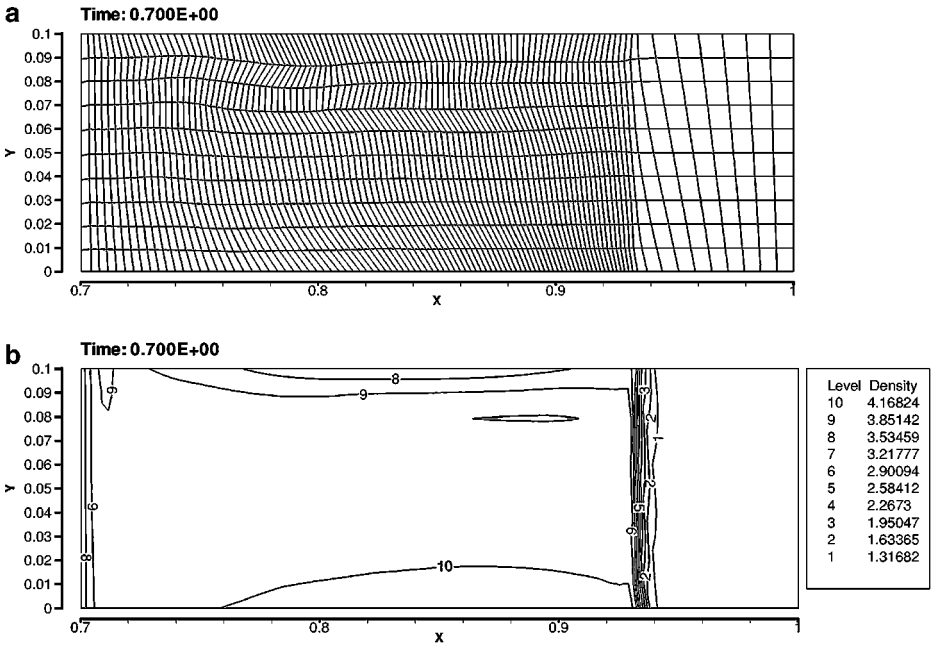

FIG. 13. Saltzman piston problem results for edge viscosity at $t = 0.7$, no subzonal pressures. (a) Grid. (b) Density contour plot.

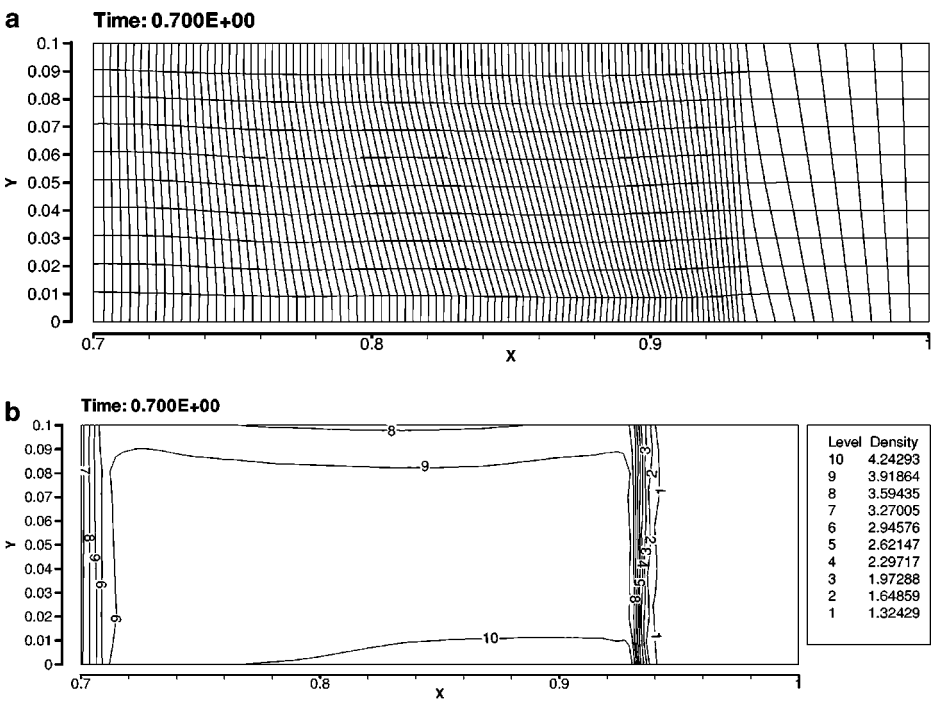

FIG. 14. Saltzman piston problem results for tensor viscosity at $t = 0.7$, no subzonal pressures. (a) Grid. (b) Density contour plot.

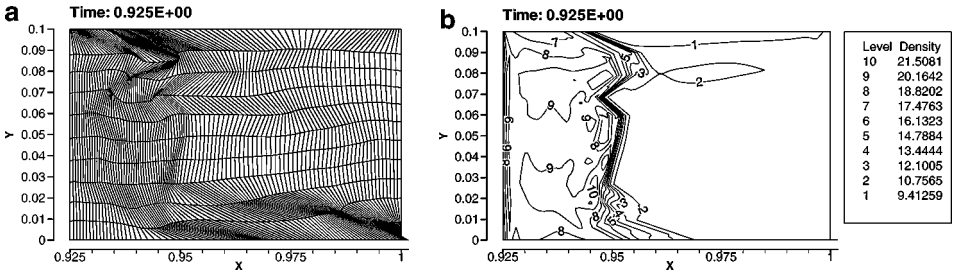

FIG. 15. Saltzman piston problem results for edge viscosity at t = 0.925, no subzonal pressures. (a) Grid. (b) Density contour plot.

of zones that are short and wide with respect to the shock direction, with an aspect ratio of 1 : 10.

Both viscosities give good results for the Saltzman piston problem at time 0.7 (Figs. 13–14). The grid is more regular for the tensor viscosity; when the calculation continues to time 0.925, this smoother grid gives improved results. Figure 15 shows the edge viscosity results at time 0.925, the grid has become uneven, and the shock wave is no longer planar. The grid is close to buckling as it contains subzonal corner volumes that have inverted, but no entire zone has inverted. The tensor viscosity results for time 0.925 show a smooth grid, and a shock that is planar everywhere except near the upper boundary (Fig. 16). Adding subzonal pressures would improve the smoothness of the grid for both viscosities.

We also used a variant of the Saltzman problem where the height of the initial grid (Fig. 12) is reduced from 0.1 to 0.025. The initial grid is generated using Eq. (53) with $dx = 1/100$ and $dy = 0.025/10$. Now the shock wave is traveling through zones that are long and thin with respect to the shock wave; the zones have an aspect ratio of 4 : 1. This is another problem where the edge viscosity causes large nonphysical grid distortions to occur (Fig. 17). The tensor viscosity retains a smooth grid and the correct shock location (Fig. 18). Compared with the results for the standard Saltzman problem, the density error at the upper and lower boundaries has increased.

6.3. Sedov Blast Wave Problem

The Sedov blast wave problem [16] models the expanding wave generated by an intense explosion in a perfect gas, an example of a diverging shock wave. The initial grid is

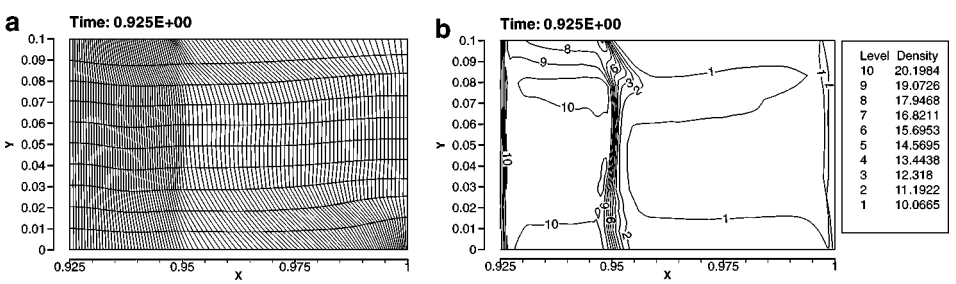

FIG. 16. Saltzman piston problem results for tensor viscosity at t = 0.925, no subzonal pressures. (a) Grid. (b) Density contour plot.

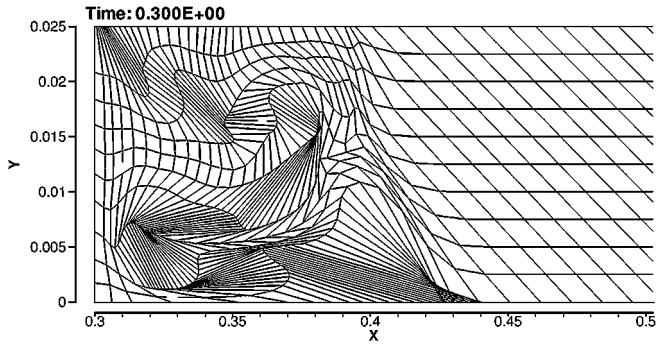

FIG. 17. 4 : 1 Saltzman piston problem grid for edge viscosity at t = 0.3, merit factor = 0.1. In this version of the piston problem the edge viscosity produces a highly distorted mesh.

rectangular, consisting of 45 × 90 zones with a total edge length of 1.1 in both directions. The initial internal energy is zero except for the two zones closest to the origin, which have a specific internal energy of 409.7. These two zones form a square, so the initial conditions are symmetric about the 45° line. The analytic solution gives, for $\gamma = 1.4$, a shock at radius unity at time unity, and with a peak density of 6.0. The numerical solution should retain the symmetry about the 45° line of the initial conditions. As the initial grid is rectangular and so not symmetric about this line, this problem provides a test of the ability of the code to maintain the symmetry of the flow when the computational grid does not embody this symmetry.

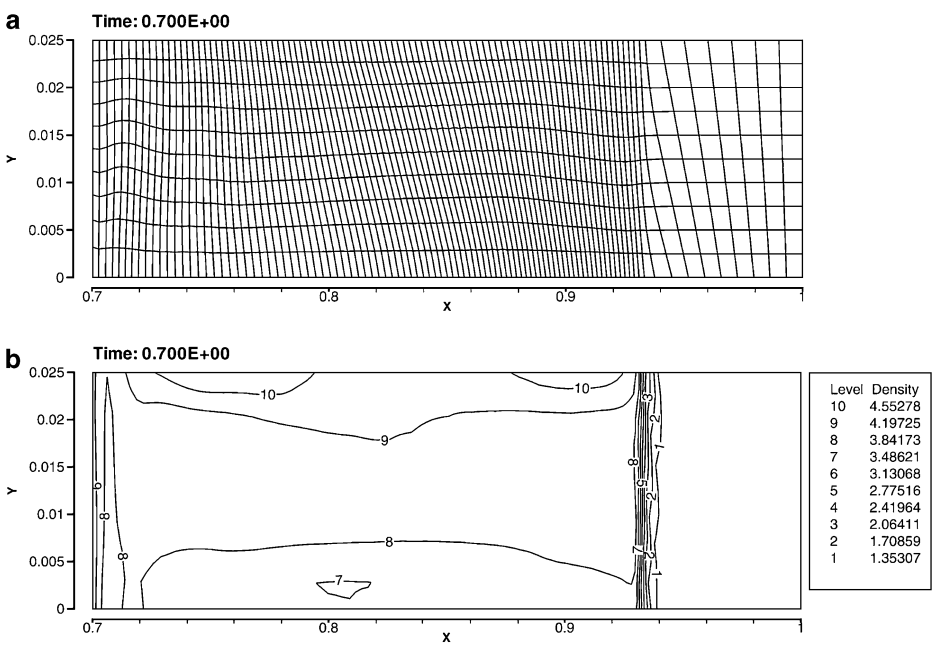

FIG. 18. 4 : 1 Saltzman piston problem results for tensor viscosity at t = 0.7, no subzonal pressures. (a) Grid. (b) Density contour plot.

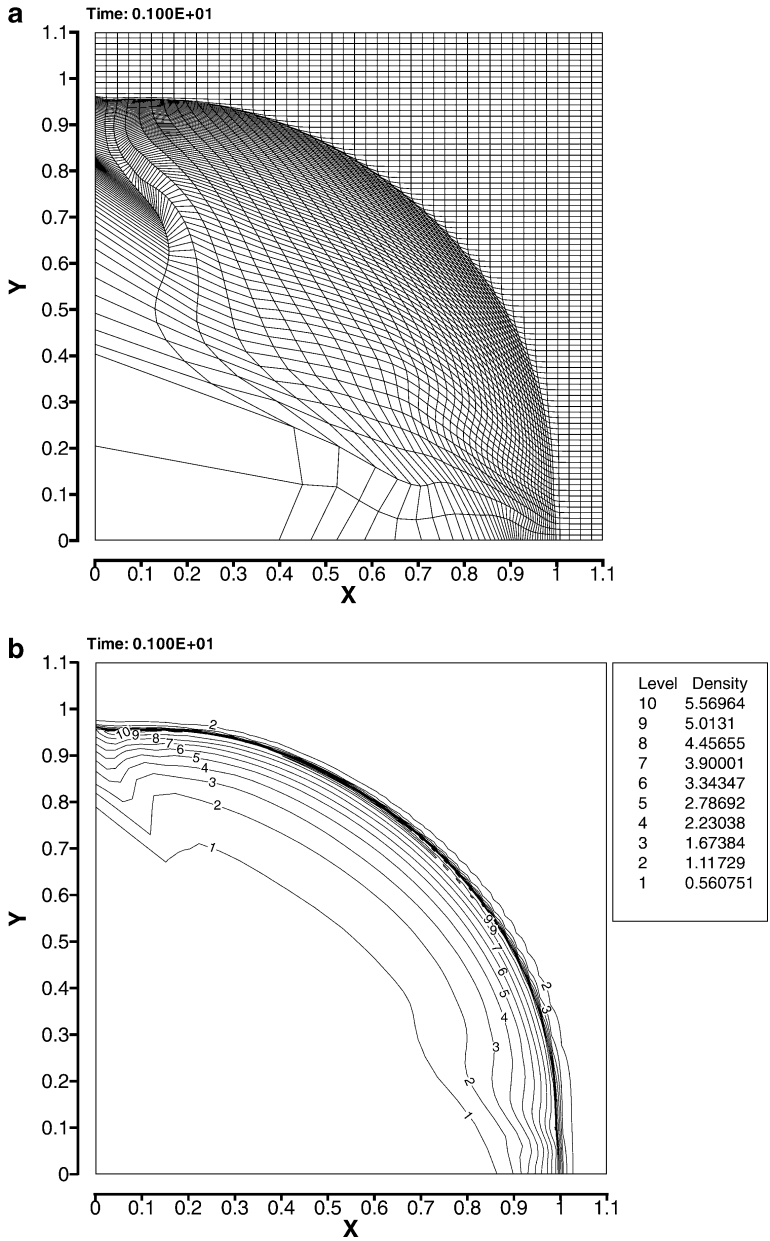

FIG. 19. 1 : 2 Sedov problem results for edge viscosity, merit factor = 0.1. (a) Grid. (b) Density contour plot.

The results shown for both viscosities were generated using subzonal pressures, using a merit factor of 0.1. Without subzonal pressures, the final grid for both viscosities includes nonconvex zones near the origin. Subzonal pressures were used to maintain the quality of the grid near the origin.

The edge viscosity now gives an elliptical shock front, with a larger radius along the x-axis (45 zones) than the y-axis (90 zones) (Fig. 19). The tensor viscosity gives a smooth grid but unlike the edge viscosity retains a circular shock (Fig. 20).

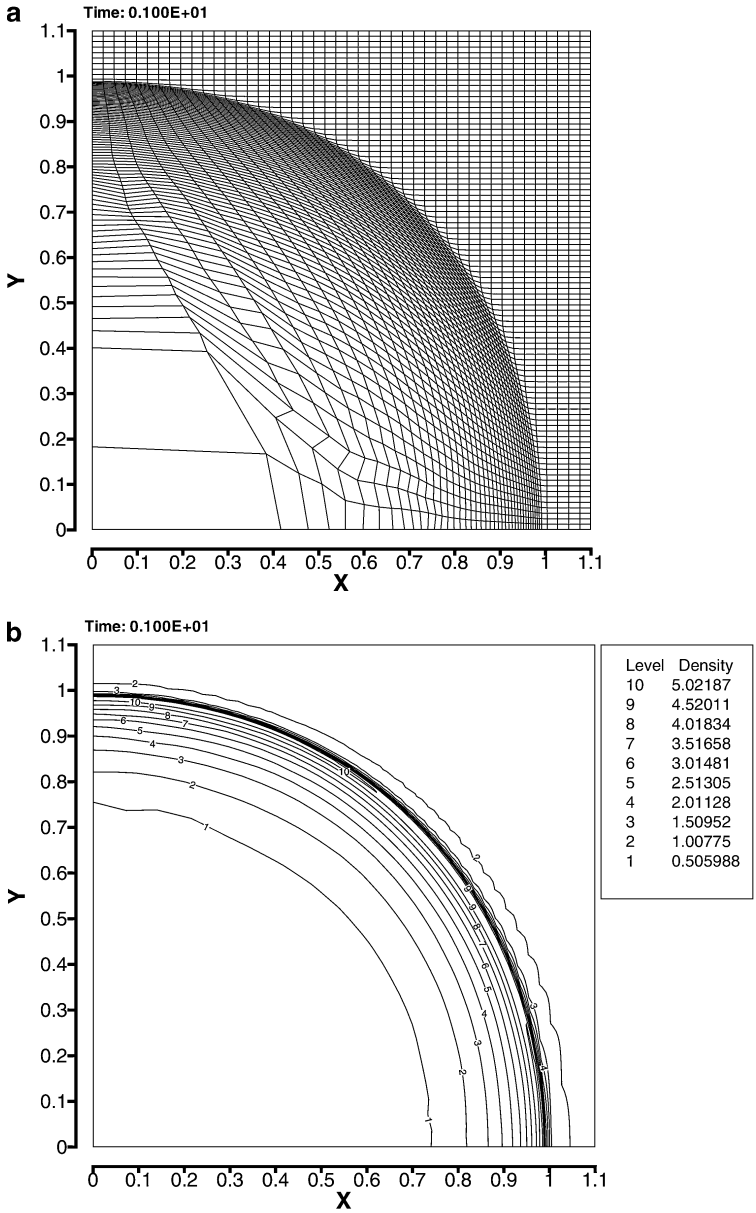

FIG. 20. 1 : 2 Sedov problem results for tensor viscosity, merit factor = 0.1. (a) Grid. (b) Density contour plot.

7. CONCLUSION

We have developed a new two-dimensional tensor artificial viscosity. The formalism consists of a scalar viscosity coefficient and discrete operators for calculating the gradient of velocity and the divergence of the viscosity tensor. The viscosity multiplies the gradient of velocity tensor to produce the viscosity tensor.

The viscosity satisfies all but one of the conditions set out by Caramana *et al.* [7]. The condition not satisfied is viscous force continuity, which states that the viscous force should go to zero smoothly as compression vanishes. As the viscosity coefficient contains the speed

of sound, it does not go to zero smoothly. The condition can be satisfied by removing the linear viscous term, but this makes the viscosity solely quadratic and results in oscillations behind shock waves. We choose not to satisfy the viscous force continuity condition in order not to introduce these oscillations.

Because of the tensor nature of the new viscosity, simulations have a reduced dependence on the relation of the grid to the flow structure. This is seen most clearly in results for the Noh problem on an initially square grid, and for the 4 : 1 Saltzman piston problem. For both these problems, the tensor viscosity results show a smooth grid, while the edge viscosity produces a highly distorted grid. In the standard Saltzman piston problem, the tensor viscosity gives a smoother grid, which results in an improved solution once the shock reflects from the fixed end of the piston. For the Sedov problem on an initially rectangular grid, the tensor viscosity maintains the expected symmetry of the shock wave.

We have extended the mimetic discretization approach for general grids to tensor operators, deriving expressions for the gradient of a vector and divergence of a tensor. We have used these discrete operators in the artificial viscosity. These operators can be used for any application where the gradient of a vector and divergence of a tensor are required.

An important area for future work is to develop and test new formulations of the viscosity coefficient and limiter function, as our tests have shown that these can have a strong effect on the results. These studies should focus on developing forms of the coefficient that fully satisfy the viscous force continuity condition.

ACKNOWLEDGMENT

We thank E. Caramana and L. Margolin for their useful comments and suggestions. This research was supported by the Department of Energy, under contract W-7405-ENG-36.

REFERENCES

1. D. J. Benson, A new two-dimensional flux-limited shock viscosity for impact calculations, *Comput. Methods Appl. Mech. Eng.* **93**, 39 (1991).
2. D. J. Benson and S. Schoenfeld, A total variation diminishing shock viscosity, *Comput. Mech.* **11**, 107 (1993).
3. J. C. Campbell and M. J. Shashkov, A compatible Lagrangian hydrodynamics algorithm for unstructured grids, LA-UR-00-3231, submitted for publication, available at http://math.lanl.gov/shashkov/
4. J. C. Campbell, J. M. Hyman, and M. J. Shashkov, Mimetic finite difference operators for second-order tensors on unstructured grids, *Comput. Math. Appl.* in press.
5. E. J. Caramana, D. E. Burton, M. J. Shashkov, and P. P. Whalen, The construction of compatible hydrodynamics algorithms utilizing conservation of total energy, *J. Comput. Phys.* **146**, 227 (1998).
6. E. J. Caramana and M. J. Shashkov, Elimination of artificial grid distortion and hour-glass type motions by means of Lagrangian subzonal masses and pressures, *J. Comput. Phys.* **142**, 521 (1998).
7. E. J. Caramana, M. J. Shashkov, and P. P. Whalen, Formulations of artificial viscosity for multi-dimensional shock wave computations, *J. Comput. Phys.* **144**, 70 (1998).
8. R. P. Fedkiw, A. Marquina, and B. Merriman, An isobaric fix for the overheating problem in multimaterial compressible flows, *J. Comput. Phys.* **148**, 545 (1999).
9. J. M. Hyman and M. Shashkov, Adjoint operators for the natural discretizations of the divergence, gradient and curl on logically rectangular grids, *Appl. Numer. Math.* **25**, 413 (1997).
10. J. M. Hyman and M. Shashkov, Natural discretizations for the divergence, gradient and curl on logically rectangular grids, *Comput. Math. Appl.* **33**, 81 (1997).

11. V. F. Kurapatenko, in *Difference Methods for Solutions of Problems of Mathematical Physics, I*, edited by N. N. Janenko (Am. Math. Soc., Providence, 1967), p. 116.
12. R. Landshoff, A Numerical Method for Treating Fluid Flow in the Presence of Shocks, Technical Report LA-1930 (Los Alamos National Laboratory, 1955).
13. L. G. Margolin, A Centered Artificial Viscosity for Cells with Large Aspect Ratios, Technical Report UCRL-53882 (Lawrence Livermore National Laboratory, 1988).
14. W. F. Noh, Errors for calculations of strong shocks using an artificial viscosity and an artificial heat flux, *J. Comput. Phys.* **72**, 78 (1987).
15. W. J. Rider, Revisiting wall heating, *J. Comput. Phys.* **162**, 395 (2000).
16. L. I. Sedov, Similarity and Dimensional Methods in Mechanics (Academic Press, New York, 1959).
17. M. Shashkov and S. Steinberg, Solving diffusion equations with rough coefficients in rough grids, *J. Comput. Phys.* **129**, 383 (1996).
18. J. Von Neumann and R. D. Richtmyer, A method for the calculation of hydrodynamic shocks, *J. Appl. Phys.* **21**, 232 (1950).
19. M. L. Wilkins, Use of artificial viscosity in multidimensional fluid dynamic calculations, *J. Comput. Phys.* **36**, 281 (1980).